Analysis of High Load Turbine Blades at Low Re Numbers with CFX-BladeGen Plus

H. Perez-Blanco
Penn State
Robert Van Dyken
Tom Mc Laughlin
Aaron Byerley
USAF Academy

Abstract

Gas turbine blades, especially those with high camber, exhibit flow separation in the suction side at part-load conditions. These conditions may arise due to reduced power demand in stationary applications, or due to flight at high altitudes. In the latter case, the reduced density compounds the lower operating velocities required to enhance range, and small trough-flows result in separation. When the inlet velocity is reduced to the point that the flow is laminar, the flow in the suction side does not embody enough kinetic energy to prevent flow reversal. Hence, a separation bubble takes place. The ensuing reduced blade effectiveness results in losses that increase fuel consumption. It has been shown experimentally in cascades that the inception and extent of separation are respectively a weak and strong function of the flow Reynolds no. Also, cascade experimental data are available in the form of pressure and loss coefficients. The flow around a highly loaded blade is modeled with CFX-BladeGen Plus. The insights thus gained regarding wake flow and surface pressures are discussed in relation to data and conclusions afforded from other experimental and analytical work. The experience with the predictive possibilities of numerical techniques regarding this difficult problem, along with the benefits accrued via simulation are addressed.

Introduction

Some turbine blade designs exhibit suction side flow separation at part load conditions, which arise at reduced power demand in stationary applications, or during flight at high altitudes. In the latter case, the reduced density compounds the lower operating velocities required to enhance range, and small trough-flows result in separation, (Fig 1).

This phenomenon is common to many low-pressure, highly loaded blades (Bons (2002)). Separation results in departures from the desired flow patterns, reducing the blade ability to extract work from the flow. Separation then increases fuel consumption. When the inlet velocity is reduced to the point that the flow is laminar, the suction-side flow does not embody enough kinetic energy to prevent flow reversal. Hence, a separation bubble takes place. The inception and extent of separation are a respectively a weak and strong function of the flow Reynolds no (Re), (List (2003)). For instance, the inception of separation takes place at nearly the same point (su/Bx equal to 1.2, Fig 1) for all Re numbers of interest, but the separation region extends further downstream at low Re numbers. This has been demonstrated with laser thermal tufts in previous publications (Byerley (2002), List (2003)).

Even though most of reported work concerning separation is of experimental nature, modeling efforts have also been reported. Choi (1988) used a finite volume formulation in conjunction with a q-ω turbulence model, but included laminar results in his study. Separation predictions were adequate for both flow regimes, but the location of separation was not as precise as sought. Yoo (1994) also studied cascade flows, producing further evidence of separation regions due to viscous effects in the blade suction side. The low velocities at which separation occurs make it difficult to collect detailed velocity and pressure measurements. Hence, CDF analysis helps elucidate separation location, wake flow distortion and the general nature and character of the separation bubble.

In the present work, CFX-BladeGen is used at Penn State University to gain insights and corroborate data acquired at the Air Force Academy. The CFX –Blade software allows implementation of approximate

cascade geometry, whereas the module CFX-BladeGen Plus yields screening solutions for various geometries and inlet conditions. The ease of use of the software allows a quick problem set-up, and the automatic grid generation simplifies the numerical approach significantly. The intent of the report is to

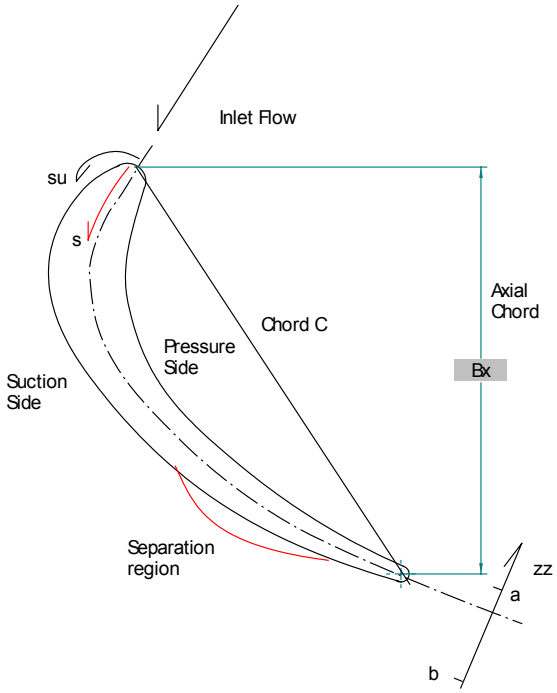

Figure 1. Blade profile, coordinates, and separation region

show that relevant information can be acquired via simulation with ease. The general trends delineated by CFX-BladeGen are compared to the general trends defined by experiment. The results can be used to plan further experiments and to shed light in the separation phenomena.

Nomenclature

α	Flow angle, deg. (Fig 2)
a	Lower limit of wake region, m.
b	Upper limit of wake region, m.
Bx	Axial chord, m
C	Blade chord, m
Cp	Pressure coefficient
$\bar{\gamma}$	Area averaged, mass flow weighted loss coefficient
d	Distance between z axis and blade centerline, m
λ	Setting angle, deg. (Fig 2)

n	Number of blades
ρ	Density, kg/m^3
p	Cascade blade pitch or pitch at mean radius, m
p_i	Static pressure at location I of the blade surface, m
p_{ti}	Total pressure at location i, Pa
Re	Cascade Reynolds no., V1·Bx/υ
Rm	Mean radius, m
s	Distance along blade centerline, m
su	Distance along suction side , m
σ	Solidity ratio, c/p.
t	Normal blade thickness, m
τ	Angle between chord and flow direction, deg. (Fig 2)
ν	Kinematic viscosity, m^2/s
V_1	Inlet cascade velocity, m/s
V_2	Velocity at exit plane (0.3 of chord from TE), in potential region, m/s
x,y,z	CFX coordinate system
xb,yb	Reference coordinate system for blade data.
zz	Cascade traverse path, m

Procedure

For meaningful modeling, the alignment of flow and simulated blades must reflect the experimental alignment. In the cascade (Fig 2), the setting angle is λ, and the flow direction is defined by α. The chord line and the flow must form the same angle τ in simulation and experiment. Likewise, considering that the line normal to the cascade leading edge coincides with the centerline (z axis in CFX), the angles α and λ must be transported to the numerical model. Accurate transport of α and λ ensures that the angle τ is indeed the same in simulation and experiment.

The blade coordinates are available in the xy plane, as depicted in Fig 3. The xy coordinate data are included in the Appendix. For simulation we choose to input the position of the blade centerline and the blade thickness. The blade centerline is entered in cylindrical coordinates. To determine the centerline position, the coordinates xc, yc of the centerline are determined by simply averaging the y surface blade coordinate corresponding to the same blade x coordinate. Then the equation of the z axis (Fig 3, coincident in direction with the normal to the cascade leading edge line of Fig 2) is formulated in the x,y system. The z coordinate is incremented from zero to the axial chord value, namely 171 mm. At each z position, the value of the angular CFX-BladeGen cylindrical coordinate is given, neglecting curvature effects, by

$$\theta = a\sin\left(d \diagup Rm\right) \qquad (1)$$

where d, namely the distance between z and (xb,yb) is acquired via the following Eq. 2

$$d = \sqrt{(xb - xzb)^2 + (yb - yzb)^2} \qquad (2)$$

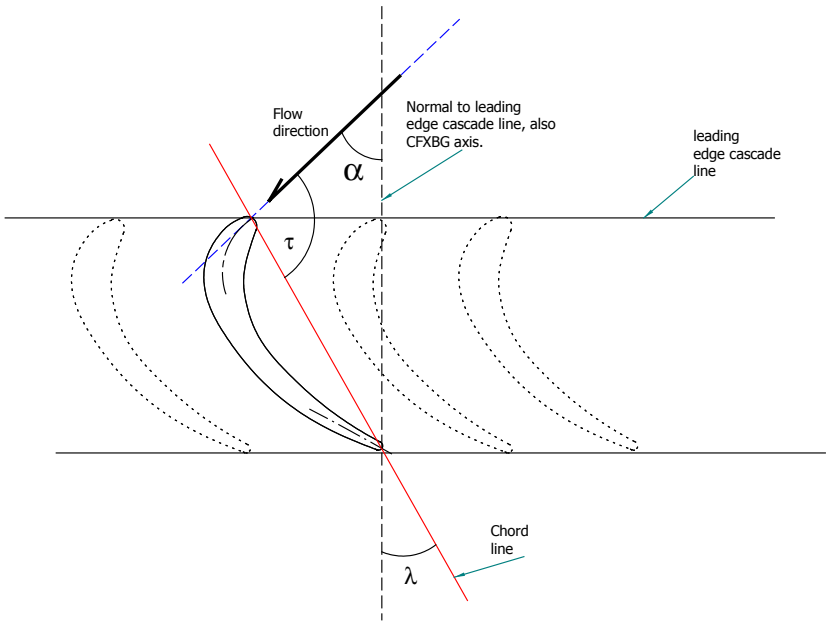

Figure 2. Schematic of cascade angles

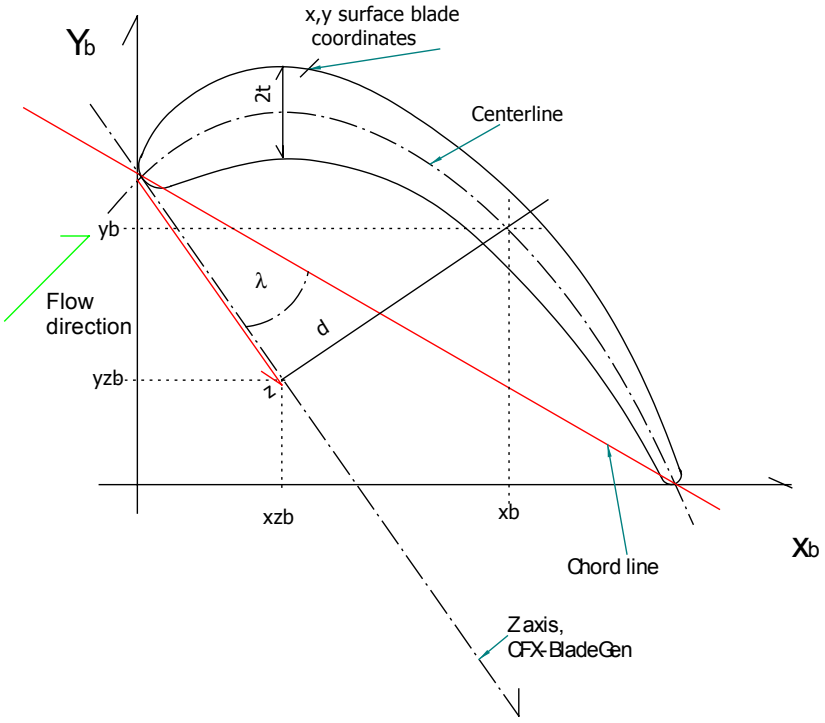

Figure 3. Schematic illustrating the definition of the distance d, between the z-axis and the blade centerline, at given z position

At each Z position, the blade thickness is obtained from measurements carried out on a 1:1 drawing of the cross-section of the blade.

The mean radius is specified as follows. Since the software assumes circular symmetry around the z-axis, an exact model of a cascade would require an infinite radius. A finite radius is instead specified, taking into account that there is maximum allowed number of blades (i.e.240) and that it is desired to vary the solidity ratio. For the solidity ratio corresponding to the cascade of the Air Force Academy, the mean radius, number of blades and pitch are related by:

$$n = 1 + \frac{2 \cdot \pi \cdot Rm}{p} \qquad (3)$$

For the maximum possible radius, the number of blades cannot exceed 240. In our case, we adopt a radius of 3087 mm, with a pitch of 163 mm and 120 blades. In general, Eq. 3 is used with the values of Table 1 to specify the number of blades at the mean span. The mid-span layer is set-up to receive the thickness and centerline angular coordinate. One remaining variable, namely the blade span, is chosen to match that of the AFA cascade. Additional layers along the span (i.e. root and tip) are generated by transferring the centerline coordinate and blade thickness from the mid-span data. An acceptable 2-D blade is thus obtained, Fig 4.

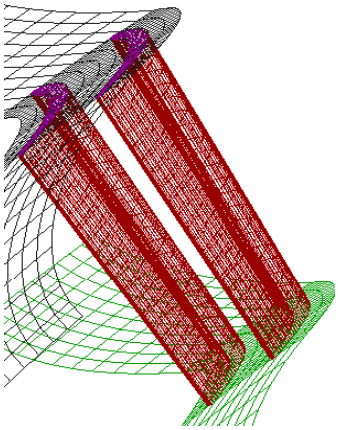

Figure 4. CFX-BladeGen+ View of analyzed blades

Table 1. Blade data

Variable	Value
Axial chord	0.171 m
Chord	0.195 m
Setting angle	28.7 deg
Rm	3.0 m
Pitch	0.163 m
Aspect ratio	4
Number of blades	115

The blade geometry thus determined is used as input to CFX-BladeGen via the command "read segment points" under "Segment operations." We find this expedient way to input blade geometry most convenient. The dimensions are entered with the dialog panel that appears when a new model is specified. This panel also allows specification of key angles to approximately fashion the blade. This feature, although not used, is most convenient when initially defining a blade. The LE and TE of the blade are closed by specifying elliptic ratios of one for both ends, this is, closing the ends with circles.

Operating conditions are specified to match the Cascade Reynolds (Re= V1·Bx/ν) number, which in this case means matching the velocity, for chord and viscosity are the same. Other operating variables are summarized in Table 2.

The solution control parameters are left to the software, and are shown in the last three lines of Table 2. Variations on the grid coarseness (not attempted in all cases) do not yield apparent changes on the results.

Table 2. Operating parameters

Variable	Value
Fluid Type	Incompressible
Fluid Description	Air at STP
Density	0.94 kg/m^3
Fluid Model	Laminar
Dynamic Viscosity	1.79e-005 N-s/m^2
Run Specification	Mass flow Exit
Inflow Swirl Angle	-47.0 deg
Inlet Total Pressure	79000 Pa
Inlet Total Temperature	300.0 K
Total Mass Flow Rate	26.0 kg/s
Wall Roughness	Smooth
Solution Control	1.0 (Most Accurate)
Solution Time step	Auto Compute
Target Residual	0.0001

Analysis

The insights afforded by numerical modeling are analyzed from two perspectives: one is to study separation for varying solidity ratios, while keeping the other variables constant. The second perspective is to study losses and Cp distribution for the actual cascade solidity ratio. The losses in the cascade are evaluated from the loss in stagnation pressures between LE and TE, using the equation

$$\bar{\gamma} = \frac{\int_a^b (p_{t1} - p_{t2}(zz)) \cdot V_2 \cdot dzz}{\frac{\rho \cdot V^2{}_2}{2} \cdot \int_a^b V_2 \cdot dzz} \qquad (3)$$

The data in region 2 are collected with a traverse on the blade wake, at 0.3 of the axial chord Bx. The traverse path is shown in Fig 1 as zz. In CFX, the exit total pressure is mass averaged and the loss is estimated as

$$\bar{\gamma}_{CFX} = \frac{pt_1 - pt_2}{\frac{\rho \cdot V^2{}_2}{2}} \qquad (4)$$

The pressure coefficient admits a number of equivalent definitions, the one adopted here being:

$$Cp = \frac{p_{t,1} - p_i}{p_{t,1} - p_1} = \left(\frac{V_i}{V_1} \right)^2 \qquad (5)$$

also, note that

$$Cp = \left(\frac{V_i}{V_1} \right)^2 \qquad (6)$$

It is noteworthy that the Cp can be interpreted as the squared ratio of potential velocities at the i location. Hence, discrepancies in the velocity ratios are proportional to the square root of the Cp, which is then rather sensitive to velocity ratios. A view of two out of one hundred and twenty blades, as given by CFX-BladeGen, is shown in Fig 4.

Results & Discussion

Separation and solidity ratio

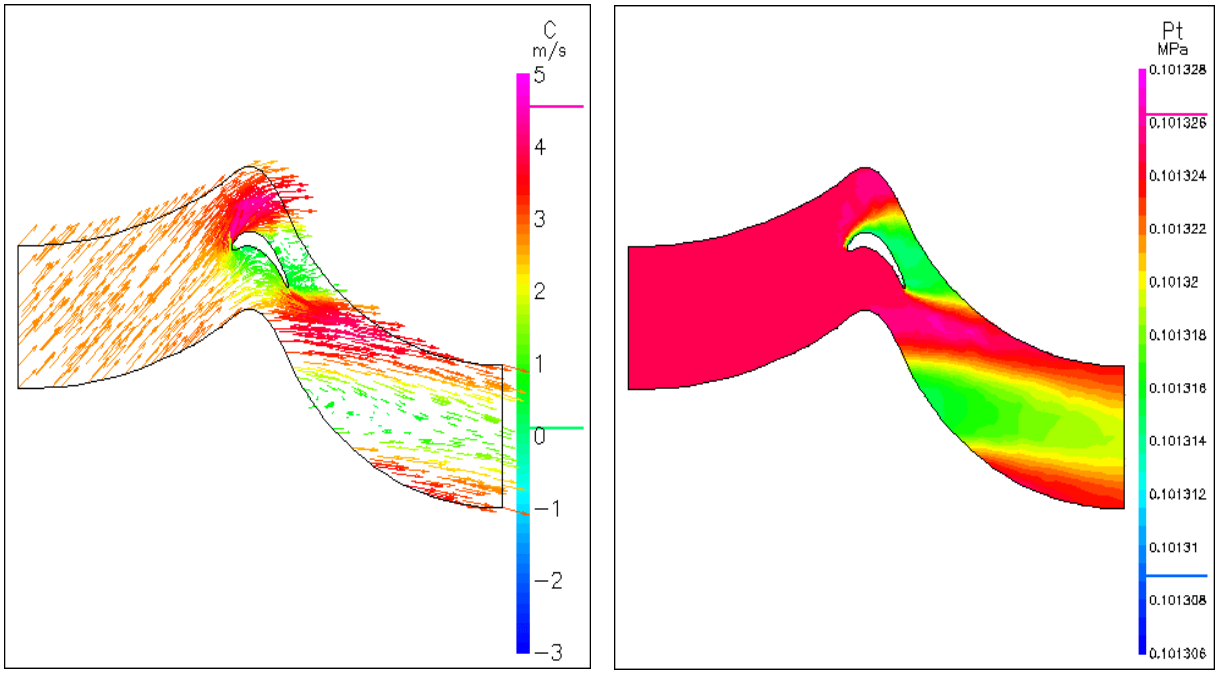

Figure 5. Velocity and total pressure distributions for σ ~0.4, 50% span

Experimental results show the location of the separation region to be approximately su/Bx~ 1 to 1.2 (Byerley 2002), where su is taken along the suction side. In the laminar regime, separation is clearly detected at low solidity ratio via numerical modeling. For instance, when the solidity ratio σ, defined as the ratio of blade chord to pitch, is ~0.4, the velocity and total pressure distributions of Fig 5 are obtained at 50% span. The velocity vector plot shows a definitive and large recirculation zone in the low-pressure side of the blade. The wake, shown for the blade below in green, is considerably disorderly due to recirculation.

The total pressure contours show a uniform region upstream, and losses of total pressure in the wake and suction side of the blade. Hence, whereas the pressure side flow is fairly reversible, the suction side is experiencing large losses, manifested in the wake.

Increasing the solidity ratio decreases the size of the recirculation region and moves it further downstream. The main characteristics of separation as evidenced in Fig 5 did not disappear, but become subtler. For instance, for an increased σ of ~0.9, a low velocity region with stagnation (i.e. velocity ~ null) exists close to the blade trailing edge, Fig 6. In any case, the laminar solution does show suction side flow behavior to be a matter of concern. This view is reinforced with the total pressure contours that exhibit relatively large losses close to the suction sidewall.

Additional insights are obtained from this part of the study: the wake region for the actual cascade flow, measured at 0.3 axial chord, would be likely to require small intervals for adequate experimental mapping, as well as certain insensitivity to flow direction for the probe used for total pressure determinations. These requirements should be taken into account when assessing the possibilities of the instrumentation for low velocity measurements, and could be instrumental for developing an accurate view of how to interpret wake losses.

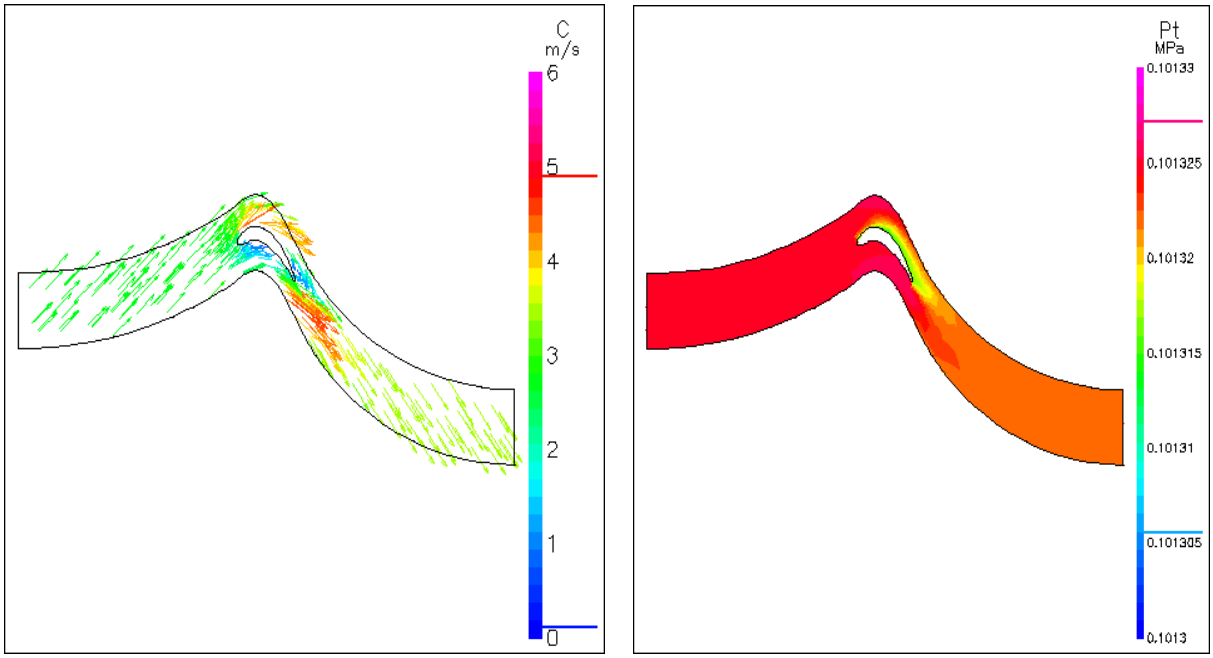

Figure 6. Velocity and total pressure distributions for σ ~0.9, 50% span

Loss and pressure coefficients

The solidity ratio of the cascade corresponds to 0.84. At this solidity, runs are completed for five different inlet air velocities, namely 3,4,5,6 and 7 m/s. The ratio of the exit potential velocity V2 to the inlet V1 ratio is plotted in Fig 7. This figure shows that as the Reynolds number increases, the theoretical prediction using laminar flow falls below the measured values. Presumably, there is an increasing turbulence level at higher Reynolds numbers, which results in thinner boundary layers, hence the reduced velocity ratio. The laminar flow specification would be expected to miss this behavior. The turbulent flow specification tends to under predict. Taken together, these are indications that a transition regime is occurring as Re increases, and that predictions should be more reliable at low Re.

The loss coefficients from CFX-BladeGen + correspond to a full pitch, whereas the wake traverse corresponds to a fraction of the pitch. The former values were adjusted by the fraction of the pitch, to adjust for the loss diffusion, and the values thus obtained are shown in Fig 8. Comparison of CFX-BladeGen+ laminar values reflects trends congruent with those discussed with reference to Fig 7. As the Re number increases, departures between experimental values and laminar theoretical values grow. The experimental values tend to approach the turbulent values, but since they do not overlap, the existence of a transition regime is apparent.

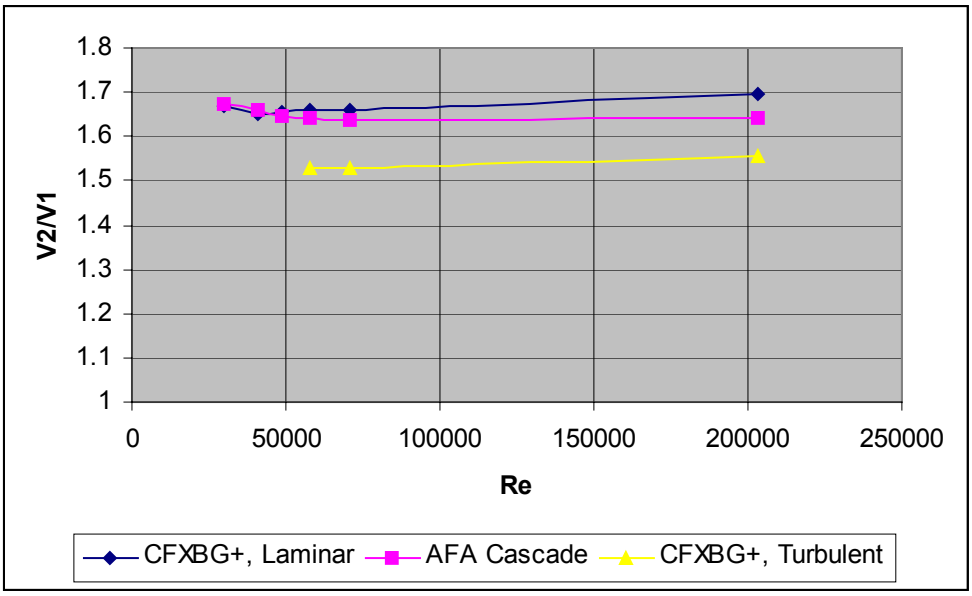

Figure 7. Velocity ratio V_2/V_1 vs. Reynolds no.

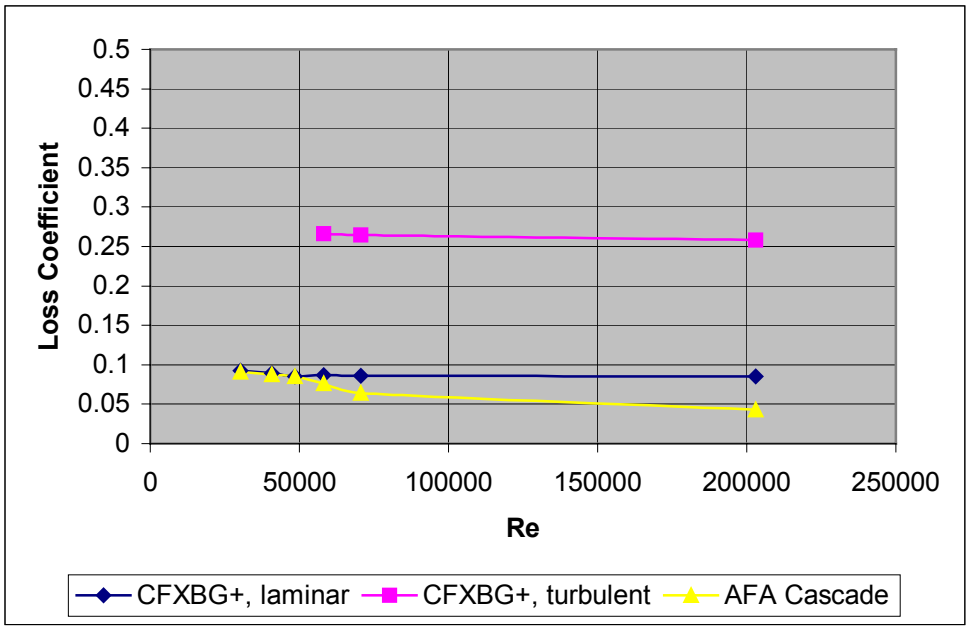

Figure 8. Loss coefficients vs. Re number

As mentioned before, the pressure coefficients magnify the ratio of potential flow velocities at a given location to the inlet velocity. Comparison of cascade Cp values to those from the simulations is not straightforward. The static pressure from the wall can be obtained form the "Loading Plot" in the Results panel. However, the streamwise coordinate, employed in this plot is, to us, of unclear geometric origin. If the pressure data are assumed to begin diverging at the blade LE, and the streamwise coordinate is measured along the blade camber line for both cascade and CFX data, the following Fig 9 is obtained.

The pressure coefficients from the cascade and software show a similar distribution in the pressure side, where the stagnation pressure losses are small. Agreement tends deteriorates close to the blade TE. These observations apply to all the Cp plots, of which we show only one here. In the suction side, the Cp peaks reach similar values at different streamwise locations.

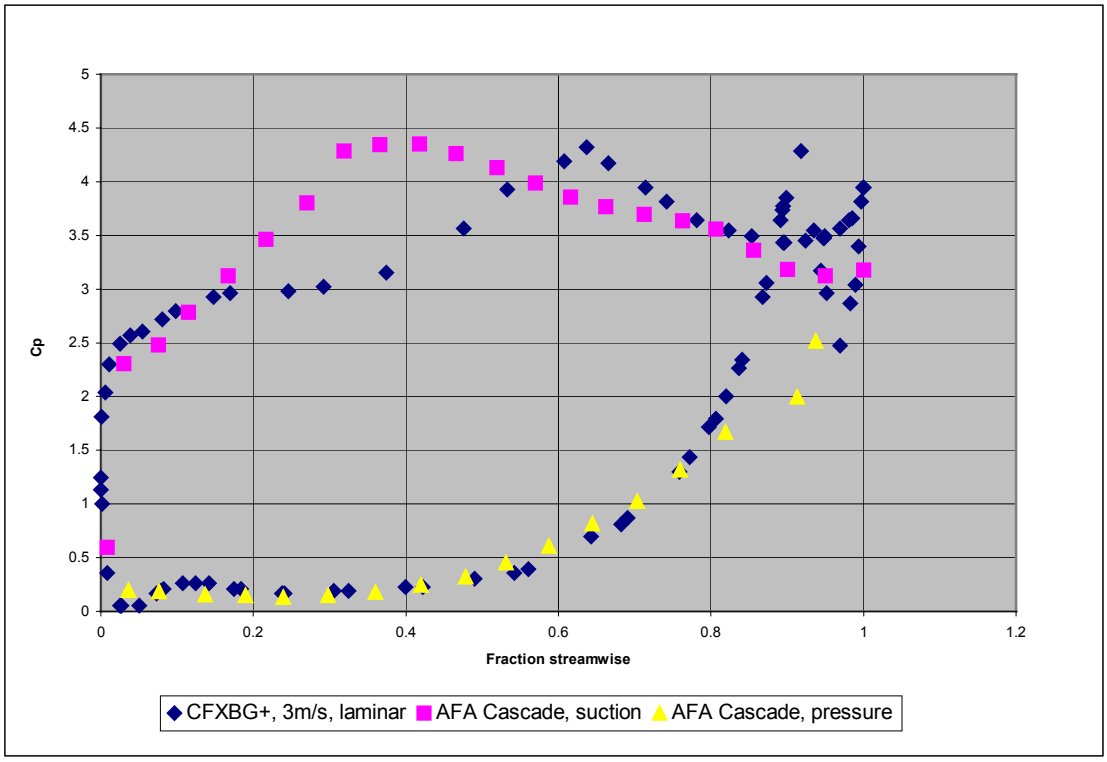

Figure 9. Pressure coefficients, 3m/s

Hence, the peak velocities in the suction side are the same, but their location differs. The region of separation has been shown to coincide with the "plateau" in the Cp distribution, present here at ~0.7 of the streamwise coordinate. Sudden increases corresponding to a sharp loss of kinetic energy are evident in the CFX-BladeGen Plus distribution, further downstream, at about 0.9 of the streamwise coordinate. The pronounced dip in the Cp in the suction side at the TE of the blade is found in the literature, and attributed to the geometrical throat of the blade being present there, in conjunction with viscous flow calculations (Yoo, 1994). The Cp predictions and measurements at low speeds appear to be quite difficult ones, as appraised from the literature. On the plus side, the Cp distributions obtained in this report are remarkably similar to the experimental ones, with the discrepancies annotated above. The suction and pressure peak velocities are quite close, and a separation region (i.e. a flat Cp region in the suction side, Byerley 2002) is evident in both distributions.

Conclusions

This work was undertaken in order to gain insights into the flow separation occurring in highly loaded blades. This situation, (or rather, its avoidance), has occupied the energies of many researchers in the experimental realm. As mere users of a remarkably easy to learn and apply CFD tool, we find numerical simulation helpful towards defining the characteristics and losses associated with wake flow for these types of blades. The integrated loss prediction agrees with measured values quite well as long as the laminar flow approximation holds true. The prediction of pressure coefficients is adequate and it resembles the measured one, but obtaining the data from the screening program version available to us may introduce some

presently unknown inaccuracies. In general, as long as the Re values are low, simulation could be helpful in the planning and result interpretation of experiments.

Loss predictions could be used to guide blade surface design. Since numerical simulation allows quick modifications of blade geometry quite effectively, it would be possible to employ this tool to study surface variations in the laminar regime that may offer an improved loss outlook. A more direct procedure for obtaining surface static pressure data from the simulation could be instrumental for such development work. Producing a model suitably reflecting the transitional flow behavior would result in further progress.

Acknowledgments

The authors wish to thank the National Academies, the Penn State Mechanical Engineering Department, CFX, and the support personnel of the AFA Aeronautics Department for enabling the outcome of the many functions that configure this work.

References

Bons J., at al. 2002. "The Fluid Dynamics of LPT Blade Separation Control Using Pulsed Jets". J. Turbomachinery, Vol 124, pp 77-85.

Byerley A. R., O. Störmer, J. W. Baughn, T. W. Simon, K. Van Treuren, J. List, 2002. "Using Gurney Flaps to Control Laminar Separation on Linear Cascade Blades," ASME Turboexpo 2002, GT-2002-30662.

Choi D., C. J. Knight. 1988. "Computation of Three-Dimensional Viscous Linear Cascade Flows" AIAA J., vol 26, no. 12, Dec 1988. pp 1477-1482.

List J., A. R. Byerley, T. E. McLaughlin, R. D. Van Dyken, 2003. " Using a Plasma Actuator to Control Laminar Separation on a Linear Cascade Blade" AIAA 2003-1026. 41st Aerospace Sciences Meeting and Exhibit. Reno, Nevada.

Yoo J. Y., J. W. Yun. 1994. "Calculation of a three-dimensional turbulent cascade flow". Computational Mechanics vol 14 (1994), pp 101-115.

Appendix

Langston Blade Coordinates, Fig 3.

#	x	y	#	x	y	#	x	y	#	x	y
1	0	4.365741	27	3.370773	4.004321	53	6.740483	0.20197	79	3.370773	5.662601
2	0.066969	4.153141	28	3.538727	3.887391	54	6.672451	0.399688	80	3.201756	5.747641
3	0.133938	4.078731	29	3.707744	3.759831	55	6.605482	0.555949	81	3.032739	5.822051
4	0.20197	4.036211	30	3.875698	3.611011	56	6.53745	0.711147	82	2.864785	5.885831
5	0.268939	4.004321	31	4.044715	3.451561	57	6.470481	0.866345	83	2.695768	5.928351
6	0.336971	3.993691	32	4.212669	3.281481	58	6.39926	1.02048	84	2.527814	5.966619
7	0.40394	3.993691	33	4.381686	3.100771	59	6.33548	1.173552	85	2.35986	5.988942
8	0.471972	4.004321	34	4.54964	2.898801	60	6.268511	1.326624	86	2.190843	5.999572
9	0.538941	4.036211	35	4.718657	2.686201	61	6.201542	1.478633	87	2.021826	5.992131
10	0.606973	4.078731	36	4.886611	2.462971	62	6.13351	1.629579	88	1.853872	5.981501
11	0.673942	4.110621	37	5.055628	2.229111	63	6.066541	1.779462	89	1.684855	5.949611
12	0.842959	4.206291	38	5.223582	1.984621	64	5.897524	2.154701	90	1.516901	5.901776
13	1.010913	4.270071	39	5.392599	1.735879	65	5.729464	2.516121	91	1.347884	5.843311
14	1.178867	4.333851	40	5.560553	1.473956	66	5.560553	2.866911	92	1.178867	5.758271
15	1.347884	4.376371	41	5.729464	1.202253	67	5.392599	3.207071	93	1.010913	5.662601
16	1.516901	4.408261	42	5.897524	0.921621	68	5.223582	3.525971	94	0.842959	5.545671
17	1.684855	4.429521	43	6.066541	0.632485	69	5.055628	3.834241	95	0.673942	5.396851
18	1.853872	4.440151	44	6.13351	0.514492	70	4.886611	4.110621	96	0.606973	5.333071
19	2.021826	4.440151	45	6.201542	0.394373	71	4.718657	4.372119	97	0.538941	5.269291
20	2.190843	4.429521	46	6.268511	0.274254	72	4.54964	4.599601	98	0.471972	5.184251
21	2.35986	4.408261	47	6.33548	0.152009	73	4.381686	4.812201	99	0.40394	5.109841
22	2.527814	4.376371	48	6.39926	0.052087	74	4.212669	4.992911	100	0.336971	5.024801
23	2.695768	4.323221	49	6.470481	0.011693	75	4.044715	5.162991	101	0.268939	4.929131
24	2.864785	4.270071	50	6.53745	0	76	3.875698	5.311811	102	0.20197	4.822831
25	3.032739	4.195661	51	6.605482	0.011693	77	3.707744	5.439371	103	0.133938	4.705901
26	3.201756	4.110621	52	6.672451	0.052087	78	3.538727	5.556301	104	0.066969	4.588971
									105	0	4.365741